SoftRafts: Floating and Adaptive Soft Modular Robots

Luyang Zhao[1*†], Yitao Jiang[1†], Chun-Yi She[1], Alberto Quattrini Li[1], Muhao Chen[2*], Devin Balkcom[1]

[1*]Department of Computer Science, Dartmouth College, Hanover, NH, 03755, USA.
[2]Department of Mechanical and Aerospace Engineering, University of Kentucky, Lexington, KY, 40506, USA.

*Corresponding author(s). E-mail(s): luyang.zhao@dartmouth.edu; muhao.chen@uky.edu;
Contributing authors: yitao.jiang@dartmouth.edu; chun-yi.she.gr@dartmouth.edu; alberto.quattrini.li@dartmouth.edu; devin.balkcom@dartmouth.edu;
[†]These authors contributed equally to this work.

Abstract

Modular robots possess great potential due to their adaptability and reconfigurability, yet their use in aquatic environments and dynamic multi-tasking scenarios—particularly for complex manipulation—remains largely underexplored. To address the need for versatile and multifunctional systems in such settings, we hypothesize that integrating soft-bending capabilities into modular robots can create a platform capable of navigating complex environments, performing diverse manipulation tasks, and assembling deformable lattices. In this work, we present a variable-stiffness soft modular robot that combines rigid 3D printed components with soft foam, utilizing a cable-actuated mechanism and a propeller. This modular robot can locomote, bend, steer, connect with other modules, and assemble into various larger active structures for different applications. For instance, when configured as a gripper, the robot can collect trash from the water's surface. When assembled into a raft, it functions as a movable platform for drone landings. In a chain configuration, the robot moves like a snake on land and transitions seamlessly to aquatic locomotion using a propeller. Additionally, these robots can operate collectively like swarm robots, such as transporting boxes collaboratively across surfaces. Our findings highlight that incorporating deformable

features into modular robot designs significantly enhances their adaptability and multifunctionality in aquatic environments.

Keywords: Modular Robot, Soft Robot, Manipulation, Locomotion, Structure Formation

When we think about modular robots, we think the robots can combine together to do more complex tasks. Soft robots offer significant potential for complex, dynamic environments due to their compliance and mechanical intelligence, especially in aquatic scenarios where they can adapt to water flow and handle fragile objects. Their application in aquatic domains remains largely unexplored. To address this gap, we present SoftRafts, a robotic platform that seamlessly integrates softness and modularity for on-water operations. Our design combines rigid 3D-printed components with soft foam, featuring a cable-actuated mechanism and propeller for untethered aquatic locomotion. The robot modules can not only connect to form complex structures for collaborative tasks (Fig. 1(i)) but also switch between soft and rigid modes, enabling unprecedented versatility. The demonstrated capabilities of SoftRafts span from amphibious navigation and diverse object manipulation to constructing deformable, variable-stiffness lattices, showcasing the unique advantages of combining soft robotics with modular design in aquatic environments.

In nature, many species, such as ants and dolphins work collectively to solve challenges related to locomotion, manipulation, or structure assembly [1–4]. For example, beavers collaborate to construct dams and lodges [1], while ants work collectively to move heavy and large objects and build rafts from their bodies to survive floods [2, 3, 5]. Inspired by such natural swarm systems, robot swarms emulate collective behavior to tackle complex tasks beyond the capability of a single robot. Modular robotics builds on this concept by enabling individual units to assemble into larger lattices, forming robots in various configurations to accomplish diverse tasks [6–8]. Significant progress has been made in terrestrial modular robots [9–11], such as SMORES [11, 12] and Sambot [13]. Recently, researchers have extended these concepts to outdoor environments, transitioning locomotion and manipulation tasks from indoor settings. Examples include snail-inspired robots [14] and multi-legged robot swarms [15].

However, research on modular robots designed for aquatic applications remains limited [8]. The majority of current aquatic reconfigurable modular robots are designed as waterborne vehicles or boats [8], excelling at tasks such as forming rigid floating platforms or enabling precise maneuverability. One notable example is a study from Yim's group in 2015 [16], which introduced the first aquatic modular reconfigurable robots. This work developed a swarm of boats, each equipped with four propellers for precise maneuverability, capable of autonomously connecting side-by-side to form larger, lattice-like structures. Another example comes from Rus' group at MIT [17], where a fleet of autonomous boats was designed to disconnect and reassemble into various configurations. These boats demonstrated the ability to form floating structures, such as rearranging three robots from a connected straight line into an "L" shape.

To expand their capabilities, incorporating soft materials into modular robot designs introduces a new dimension of adaptability and versatility. Soft materials provide compliance [18], enabling robots to conform to uneven surfaces, interact more effectively with fragile or irregular objects, and provide mechanical intelligence, which allows them to passively adapt to external stimuli, such as bending under pressure or flexing to reduce drag, thereby enhancing their ability to perform complex tasks in different aquatic environments [19]. When integrated with variable stiffness mechanisms, soft modular robots can transit between compliant states for flexibility and stiffened configurations for load-bearing or structural tasks. This dual capability enhances the functionality of existing designs, enabling new applications such as diverse manipulation tasks and merging multiple functionalities into a single platform. These robots can form adaptable floating platforms, construct deformable lattices for various manipulation tasks, perform different types of locomotion, and transform into various shapes to meet the demands of complex scenarios.

Designing waterproof, untethered, aquatic soft modular robots presents significant challenges due to the interplay of various factors that must be carefully addressed.

i) Actuation is one of the primary considerations. Different actuation methods for soft robots, such as thermal-responsive systems [9], cable-driven mechanisms [20], pneumatics [21], electrically-responsive methods [22, 23], and magnetically-responsive approaches [24], among others, offer distinct advantages and trade-offs. Enabling untethered operations while achieving essential functionalities—such as bending, steering, locomotion, and variable stiffness—poses a significant challenge in selecting the appropriate actuation method. The chosen method must balance precision, efficiency, and compactness to meet the demands of an untethered aquatic modular system.

ii) Material selection is equally crucial, as the materials must provide both softness for compliance and flexibility, as well as the ability to transition to a rigid state for load-bearing or structural tasks. Commonly used materials in soft robotics include silicone, foam, and other elastomers [25, 26], which offer a good balance between deformability and durability. However, for building multiple modules—particularly when scaling up to more than 20—the fabrication process becomes a significant factor. It must be efficient, consistent, and scalable to ensure uniformity and functionality across all modules while maintaining the desired material properties. Addressing these fabrication challenges is essential to achieve reliable performance in complex, large-scale robotic assemblies.

iii) Waterproofing and untethering present critical challenges [27, 28], particularly in cable-driven systems where delicate internal mechanisms must be safeguarded against water ingress. The direct exposure of cables to water necessitates the isolation of the winch and motor while simultaneously maintaining dynamic waterproofing to allow continuous operation. The design must ensure that actuators, cables, and electronic components remain securely sealed, providing robust protection without compromising the system's motion or overall functionality.

iv) Interconnection methods between modules are also a key challenge. The connections must enable robust attachment while ensuring the seamless transmission of forces and motion between modules [29]. This is particularly important for creating adaptable, reconfigurable systems that can form larger structures or perform collaborative tasks. The placement and design of connectors significantly influence the assembly patterns and the versatility of the system [19]. For example, to achieve all-directional connectivity, as demonstrated in StarBlocks [10], the connectors must be strategically positioned to allow for flexible reconfiguration, ensuring compatibility with a wide range of assembly geometries and operational demands.

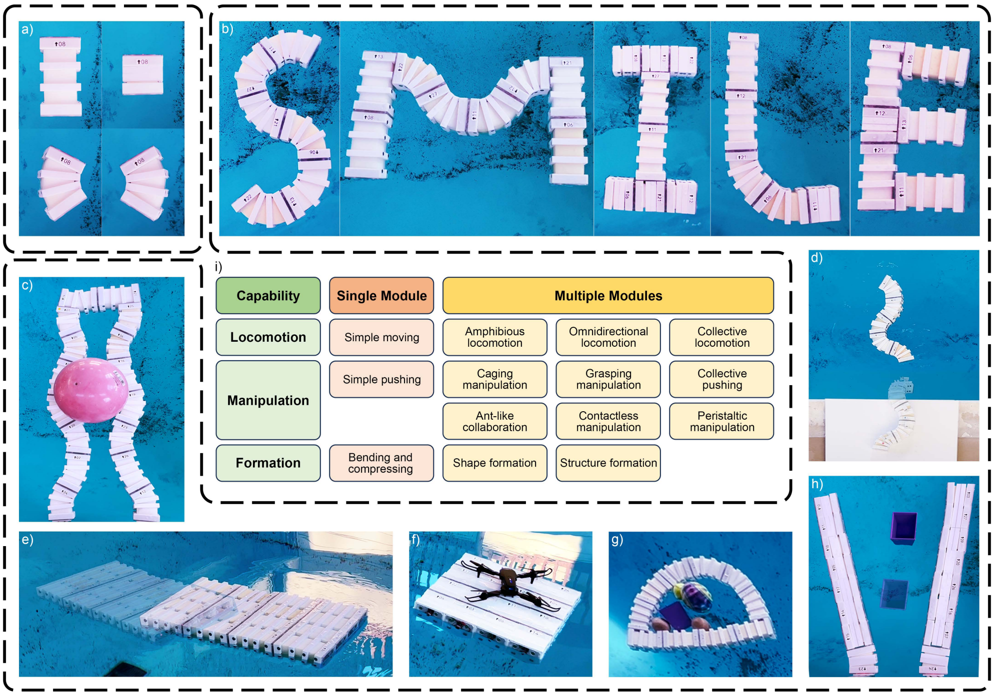

Fig. 1 Overview of the capability of SoftRaft modular robot in a single module and multiple modules. **(a)** Single module shape deformation. **(b)** Robots form 'SMILE' shapes and structures. **(c)** Two chains of modules manipulate a ball using peristaltic manipulation. **(d)** A chain of modules locomotes from the ground and gets in the water. **(e)** A raft combined with multiple modules that can move in the water. **(f)** Multiple modules formed a rigid raft structure that allows a drone to land on it. **(g)** Caging manipulation. **(h)** Water flow contact-less manipulation. **(i)** Capability table between a single module and multiple modules comparison.

In this work, we aim to advance the development of untethered, aquatic soft modular robots capable of reliable operation in dynamic environments. By enabling softness through aquatic modular robots, we address this critical gap and demonstrate the concept's potential through various application scenarios. To address the identified design challenges, we drew inspiration from the principles of push puppets to develop a cable-driven system with two strings. Each module combines 3D-printed rigid components with soft foam components and incorporates a propeller for rapid locomotion on water. By shortening strings, the robot can deform into the curve or transit from a soft, compliant state to a fully rigid state, enabling a seamless switch between tasks that require flexibility or structural rigidity. To achieve waterproofing and untethered operation, we implemented wireless charging and developed a mechanism to isolate the winch from the motor to ensure reliable performance in submerged conditions.

We evaluated the robot's capabilities across three core functionalities: locomotion, manipulation, and formation (Fig. 1(i)). For locomotion, individual modules perform simple motions, while multi-module configurations, such as chains for amphibious movement on ground and water (Fig. 1(d)) and plus-sign structures for omnidirectional navigation (Fig. 7(b)), showcase versatility. Manipulation tasks leverage configurations like caging for transporting objects (Fig. 1(g)), contactless manipulation through water currents (Fig. 1(h)), and wave-phase strategies for non-prehensile operations (Fig. 1(c)). It also able to manipulate object collectively (Fig. 5(c,d)). For formation, individual modules perform simple motions (Fig. 1(a)), while multi-module configurations, such as (Fig. 1(b)) present the shape formation and structure formation to show the word 'SMILE'. The robots assemble into rafts for drone landing platforms (Fig. 1(f)) (Fig. 4(c)), bridges for moving small vehicles (Fig. 4(d)), or carriers supporting multiple decks for aircraft operations (Fig. 4(e)). These experimental results demonstrate the versatility of the design and its enhanced capabilities when multiple modules are combined, underlining the potential of this approach for addressing diverse tasks in complex aquatic environments.

Results

Mechanism overview

Each robot in the modular system is composed of four rigid components and a soft foam core, as depicted in Fig. 2. The front and rear rigid components (Head and Tail) house the controller (printed circuit board–PCB), power supply (battery), and actuators (motors). The two middle rigid components form a structural frame that securely holds the foam core, which is chosen for its buoyant and flexible properties. This design allows the foam to compress fully within the middle rigid frames, facilitating seamless transitions between soft and rigid states while maintaining a compact structure.

The robot features three primary controllers: two motors, located within the rigid head container, which control the left and right strings to enable precise bending movements. A third motor, housed in a 3D-printed component for protection attached to the rigid head part, drives a propeller for forward and backward motion. The rear rigid container houses a sealed battery, a wireless charging module, a switch controller for power, and a power button for operation. The power cord runs from the rear components to the head components, passing through the middle of the soft foam, as depicted in Fig. 2(c1,c2). This separation design balances the mass and buoyancy along the robot.

Waterproofing the cable-driven system was accomplished by isolating the winch from the motors using a combination of a shaft seal, waterproof grease, and an acrylic (PMMA) cover, as illustrated in Fig. 2(c1). To ensure each robot is waterproof, two rubber plugs are used: one at the bottom of the rigid part of the head and the other at the tail part. Once all parts are sealed, the waterproofing is tested in two stages: static

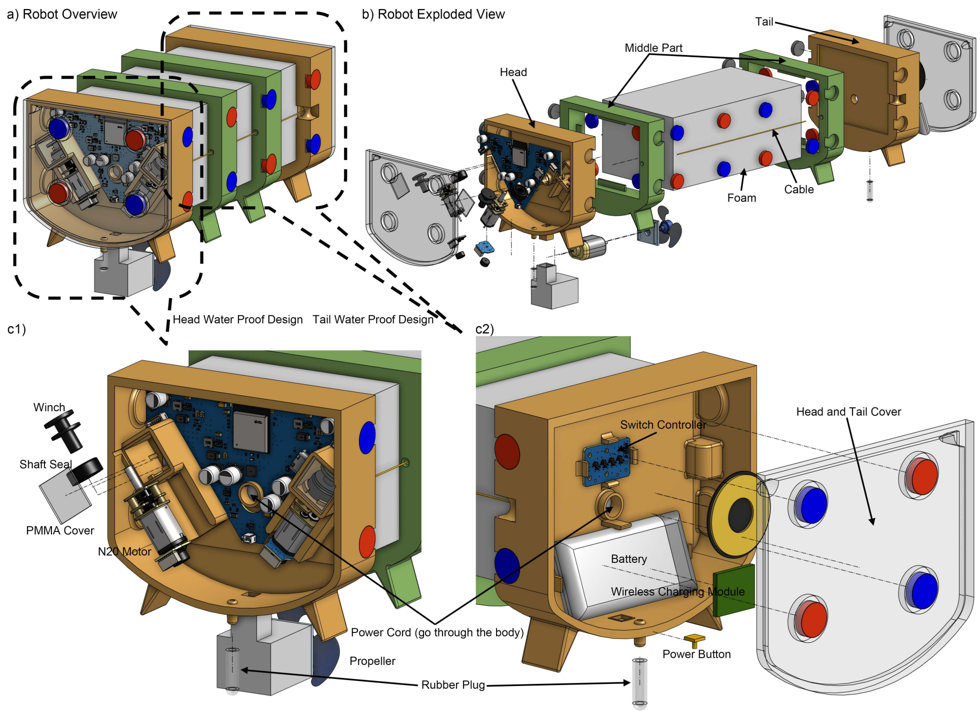

Fig. 2 Mechanism overview of a single robot. Head and Tail parts are 3D printed with resin, while the Middle parts are 3D printed with PETG. **(a)** CAD model of a complete single module. **(b)** Exploded view of a single module. **(c1)** Head part water proof design dissection, **(c2)** Tail part water proof design dissection.

and dynamic tests. In the static test, air is injected into both containers using a syringe, and the system observed approximately full rebound in the syringe, indicating a sealed environment. If the static test is successful, the robot is submerged in water and tested if any bubbles appear when pushing the air into the chamber. For the dynamic test, the propellers and motors are activated while the robot operates underwater to confirm the waterproofing under real-world conditions.

The configuration space of a single robot is determined by the lengths of two strings, s_1 and s_2, which control its deformation. The original width-to-length ratio of the robot is 1:2. The purpose of this design is can achieve symmetric attachment in both the original and compressed state. When both strings are shortened to half their original length, the robot transitions from a soft to a rigid state, allowing it to sustain a maximum load of 0.4 kg. If only one string is shortened, the robot bends to one side, enabling shape formation and steering. As illustrated in Fig. 1(a), the robot can achieve four primary states: the original state ($s_1 = s_2 = s$), bending to the left ($s_1 = \frac{1}{2}s, s_2 = s$), bending to the right ($s_1 = s, s_2 = \frac{1}{2}s$), and the compressed state ($s_1 = s_2 = \frac{1}{2}s$). Since the string lengths can vary continuously, the robot can achieve an infinite number of intermediate states, resulting in a highly versatile configuration space.

Beyond its deformation capabilities, the robot can perform locomotion and simple manipulation tasks using its propeller. A single robot's Cost of Transport (CoT) is approximately 68.35, calculated using the equation CoT = Power/(Weight · Speed), where Power = 8.66 W represents the average energy consumption, Weight = 0.384 kg is the mass of the robot, and Speed = 0.33 m/s is the robot's maximum velocity when moving forward in calm water conditions. We also designed six different motion primitives and tested how each primitive affected the robot's position and orientation to understand its locomotion capabilities. The six gaits include *forward*, *backward*, *left_front*, *right_front*, *left_back*, and *right_back*. Figure S1 shows the global x-y positions achieved by the robot under each gait, assuming an initial position and orientation of (0, 0, 0). The cluster centers for each gait are marked with stars (*), with dashed lines indicating the robot body orientation based on the average θ of the gait. The origin (0, 0) represents the robot's starting position, with a dashed black line showing its initial orientation parallel to the x-axis.

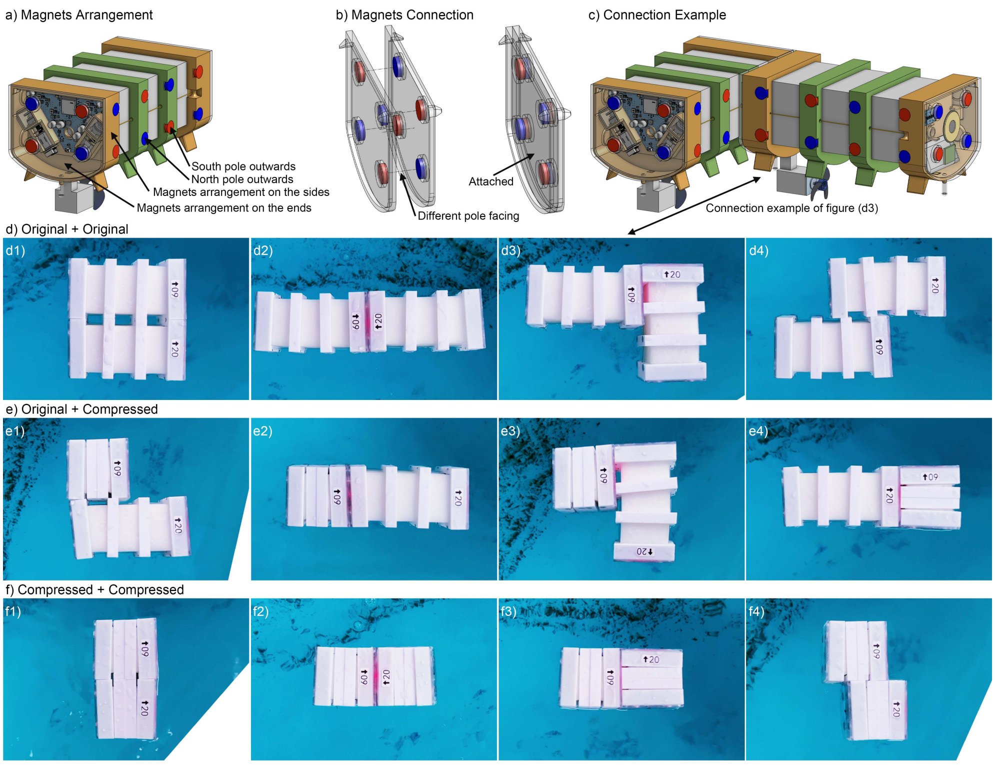

Fig. 3 Magnet arrangement and connection configurations between two modules. (a) Magnet arrangement on a single robot. **(b)** Magnet-based connection mechanism. **(c)** Example of a connection between two modules. **(d)** Four possible connection configurations when both modules are in their original state. **(e)** Four connection configurations when one module is in the original state and the other is compressed. **(f)** Four connection configurations when both modules are compressed.

Connectivity

In terms of connectivity, each robot is equipped with magnetic connectors on all four sides—front, back, left, and right—enabling versatile multi-robot configurations. The detailed magnet arrangement is shown in Fig. 3(a,b,c), which supports connections between robots from various directions (Fig. 3(d)). When compressed, the robot forms a square from a top-down view, facilitating attachments in multiple orientations (Fig. 3(e,f)). This design allows the robots to assemble into various shapes tailored for specific tasks. For example, they can form snake-like chains for locomotion on both ground and water (Fig. 7(a)), a plus-sign shape with five modules for omnidirectional locomotion (Fig. 7(b)), or larger lattice structures for manipulation and the construction of movable platforms (Fig. 4(d)). The magnetic connectors exhibit significant strength, supporting approximately 2 kg before detachment, ensuring stability and reliability in multi-robot assemblies.

Shape and structure formation

Fig. 4 Structure formation and shape formation of multiple modules. (a) A chain of modules forms an 'S' shape. **(b)** Three chains of modules form an 'I' structure. **(c)** Multiple modules form a soft raft and then compress into a rigid raft, which allows a drone to land on it. **(d)** A lot of modules form a bridge, allowing a toy car to run on it. **(e)** Multiple modules form two platforms with a flat board on it. Perform as an aircraft carrier.

Shape formation

Our modular robots can form various shapes and structures by deforming modules or through different assembly configurations (shown in Movie S1). As shown in Fig. 4(a,b), examples include forming letters such as "I" and "E" through specific arrangements and assembly methods. For a chain of robots, shapes like the letters "S" and "L" can be achieved by adjusting the string lengths of each module. The letter "M" combines both approaches: three chains are first assembled into a door-like shape, after which the middle chain deforms to complete the "M" shape. This versatility highlights the modular robots' adaptability in forming complex structures.

For a chain of modules to deform into different shapes, an analytical relationship exists between the string lengths s_1, s_2, the angle θ, and the length L of the middle curve of the robotic structure. The structure comprises four rigid 3D-printed components, denoted as r_1, r_2, r_3, and r_4, each with a length l_r. Figure S2 illustrates the geometric configuration of the structure.

In the forward kinematics process, the resulting shape of the robot chain is calculated based on the given string lengths s_1 and s_2. The equations are as follows:

For $s_1 \leq s_2$:

$$\theta = 3\cos^{-1}\left(1 - \frac{(s_2 - s_1)^2}{18 l_r^2}\right), \quad L = \frac{s_1 + s_2}{2}.$$

For $s_1 > s_2$, the angle becomes negative:

$$\theta = -3\cos^{-1}\left(1 - \frac{(s_2 - s_1)^2}{18 l_r^2}\right), \quad L = \frac{s_1 + s_2}{2}.$$

At the initial state ($s_1 = s_2 = L$), the robot remains undeformed ($\theta = 0$).

In the inverse kinematics process, the required string lengths s_1 and s_2 are determined to achieve a desired curve characterized by specific values of L and θ. The equations are:

$$s_1 = L - \frac{1}{2}\Delta s, \quad s_2 = L + \frac{1}{2}\Delta s,$$

where

$$\Delta s = \sqrt{18 l_r^2 \left(1 - \cos\left(\frac{\theta}{3}\right)\right)}.$$

If $\theta < 0$, the values of s_1 and s_2 are swapped to reflect the negative angle.

These equations establish the relationship between the string lengths, the angle θ, and the middle curve length L, enabling precise control of the robot's shape. This analytical framework allows the chain of robots to adopt a wide range of shapes tailored to meet the demands of diverse tasks. The derivation of these equations is detailed in the supplementary methods under "Kinematics of Modular Robot".

Structure formation

Our robots demonstrated their versatility by forming various lattice structures for different applications (shown in Fig. 4 and Movie S1). In one example, the robots were configured into a flat lattice structure to serve as a temporary, movable platform for drone landing, as shown in Fig. 4(c). This lattice could move omnidirectionally and compress into a rigid platform, providing a stable and adaptable surface for drone operations. In another example, the robots were assembled into a larger lattice structure to form a bridge capable of supporting the movement of a small toy car, showing the robots' ability to create structures for potential transportation tasks (Fig. 4(d)). Additionally, two separate movable platforms, each constructed with modular robots and topped with a rigid board, were joined together to simulate an aircraft carrier. This assembly, illustrated in Fig. 4(e), demonstrated the potential of scalability and adaptability of the modular robots for larger, more complex structures.

We have tested the maximum load of the robot in the rigid mode, which is designed to sustain weight. The load for a single module is about 400 g. The load can be a linear superposition with more modules.

Manipulation

Our robots are capable of various manipulation strategies to interact with and move objects. This section explores four key manipulation techniques: caging, grasping, non-prehensile manipulation, and contactless manipulation.

Caging: trash collection, transport, and enclosure

Our modular robots can form structures to surround and manipulate objects, enabling tasks such as trash collection, transport, and water enclosure. Caging stabilizes objects by forming a complete or partial enclosure. Once enclosed, the robots coordinate their movements to transport the object while maintaining the enclosure.

One example is a gripper-like caging configuration (shown in Fig. 5(a) and Movie S1), where three chains of modules are connected into a door shape. The left and right chains are used for steering and moving the structure. Control primitives allow the gripper to move forward, left, and right, enabling real-time operation for collecting and transporting trash. After the objects are collected, a fully enclosed caging mechanism ensures that all objects remain securely contained during transport.

This strategy is particularly effective for transporting irregularly shaped, fragile, or small objects that require a stable hold without direct physical contact. By maintaining the object within a stable formation, the caging approach ensures safe and efficient transport across dynamic aquatic environments.

Grasping for secure object transport

In the grasping strategy, the robots form a full loop around the object and contract inward to securely grip it. Unlike caging, grasping involves a tighter hold for greater control. Once grasped, the robots coordinate their movements to transport the object while maintaining a secure grip. (Fig. 5(b) and Movie S1) shows an example of a 2D gripper grasping a swim ring.

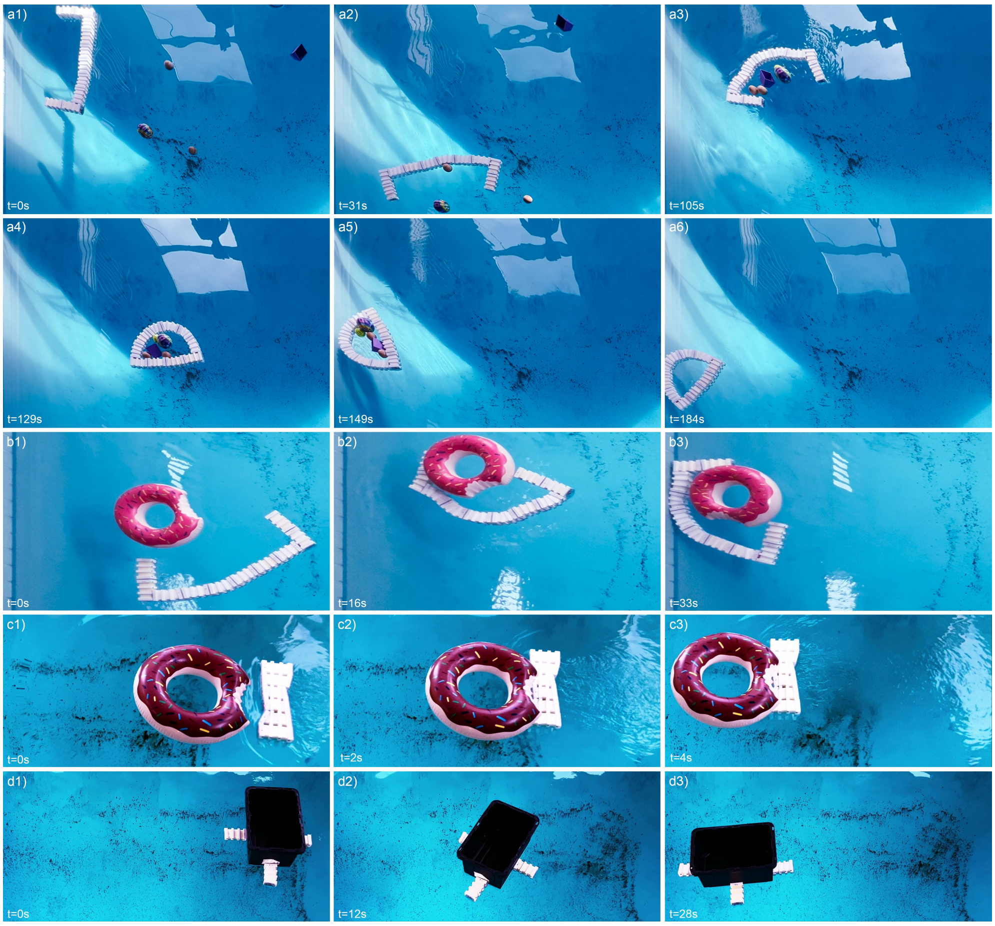

Fig. 5 Manipulation of multiple modules. (a) Caging manipulation. A robot cage formed with multiple blocks moving on the water, collecting objects floating on it, and then caging them securely. **(b)** Grasping manipulating. For large objects, the robot cage can act as a gripper and grasp the object to manipulate. **(c)** Pushing manipulation. A pile of modules deforms into the matching shape and pushes the object floating on the water. **(d)** Ant-like collaborative omnidirectional manipulation. For blocks to push the object together, by controlling the pushing force, the object can move in any direction.

Non-prehensile manipulation

Non-prehensile manipulation involves interacting with objects without fully enclosing or grasping them. Instead, this approach relies on external forces or coordinated configurations to achieve desired tasks. Our modular robotic system demonstrates two distinct non-prehensile manipulation strategies:

Multi-robot collaboration for moving large objects. Inspired by the behavior of ants moving large objects [3], multiple robots coordinate to apply synchronized forces to manipulate objects with physical contact but without physically attaching to them. This strategy enables the robots to collectively push or pull large objects, such as boxes or swim rings, by leveraging distributed force application. Fig. 5(d) and Movie S1 illustrates an example where four modules work collaboratively to push a box in different directions. To maintain contact with the box without physically attaching to it, the propellers of all modules are carefully controlled. For instance, if robots A, B, C, and D are arranged clockwise, moving the box toward robot A requires the propellers of robots A, B, and D to operate at low speed to maintain contact, while robot C increases its propeller speed to generate the required net force toward robot A. Another example, shown in Fig. 5(c) and Movie S1, involves a chain of modules connected side-by-side to push a swim ring. The modules deform to better fit the shape of the swim ring, and propeller control is used to steer and move the entire chain.

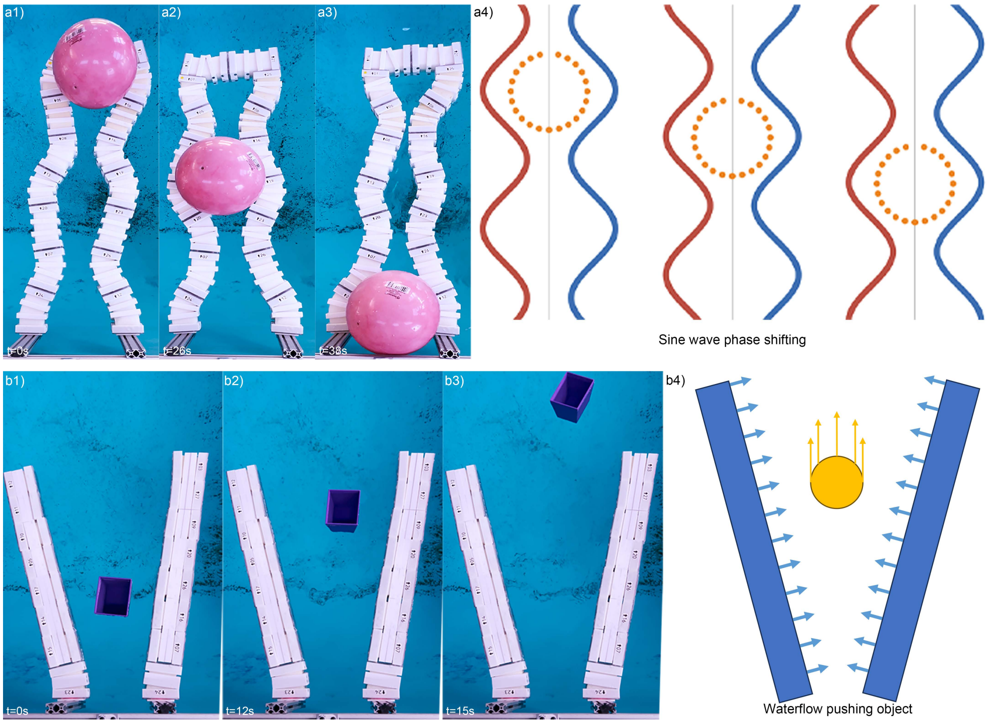

Fig. 6 Manipulation with two chains of robots. **(a)** Wave phase changing non-prehensile manipulation. The robot squirms with the Sine wave pattern to manipulate the ball. **(b)** Water flow contactless manipulation. The robot uses propellers to create water flow, which can manipulate objects.

Peristaltic manipulation. This method uses two parallel chains of robots to generate wave-like contractions for moving objects. The motion is achieved by sequentially tightening and relaxing the string lengths of each module, producing a wave-like deformation similar to biological peristalsis. To implement this, one chain of robots is fitted to a sinusoidal curve, described mathematically as $y = \sin(x + t)$, where t represents a phase shift over time. The second chain mirrors this curve symmetrically across the middle axis. The sinusoidal motion is discretized into six distinct stages per period, corresponding to evenly spaced phase shifts of $\frac{\pi}{3}$ radians (60°). Each stage determines the desired string lengths s_1 and s_2 for each robot in the chain. These lengths are computed based on the required deformation to match the sinusoidal shape, as derived from the inverse kinematics equations. By iterating through these stages, the chains generate a traveling wave that applies periodic pressure to objects positioned between them, propelling the object forward.

The sequence of six stages ensures a continuous wave motion, with each robot transitioning smoothly between states to maintain a stable and consistent force on the object. This method is particularly effective for manipulating objects through narrow spaces or over uneven surfaces, as the wave motion dynamically adjusts to accommodate irregularities. Fig. 6(a) and Movie S1 illustrates the stages of the wave-like motion and the corresponding deformation of the robot chains.

Contactless manipulation

Contactless manipulation involves moving objects by generating water currents rather than through direct physical contact. As shown in Fig. 6(b) and Movie S1, two chains of robots can form a tunnel to create a directed water current. This controlled flow transports objects without direct interaction, with each robot contributing to the stability and consistency of the current. The tunnel method operates similarly to the concept of a fish ladder, where a controlled current guides objects through the tunnel with precision and consistency.

Locomotion

Our modular robots can achieve diverse locomotion strategies by adopting different configurations and control approaches tailored to specific environments and tasks. The arrangement of modules determines the propulsion mechanism and the control strategy required for efficient movement. For example, chain configurations enable both amphibious locomotion and adaptability in transitioning between ground and water, while symmetrical arrangements like the plus-sign configuration allow for omnidirectional movement with precise control. Below, we present two examples illustrating how these configurations are optimized for distinct locomotion tasks.

Amphibious locomotion using a chain of modules

Inspired by the undulatory gait of snakes, we developed a gait for ground locomotion that achieves diagonal forward motion through coordinated and asymmetric lateral bending, similar to gaits used in other snake robots [30, 31]. In this method, five modules are connected into a chain, as shown in Fig. 7(a) and Movie S1. The gait alternates between bending modules 1, 2, and 5 in one direction (e.g., left) and modules 3 and 4 in the opposite direction (e.g., right), creating an unbalanced wave-like motion. This actuation sequence is then reversed, with modules 1, 2, and 5 bending to the right and modules 3 and 4 to the left. The asymmetric pattern introduces mechanical imbalance, which propels the robot diagonally forward, even on surfaces with isotropic

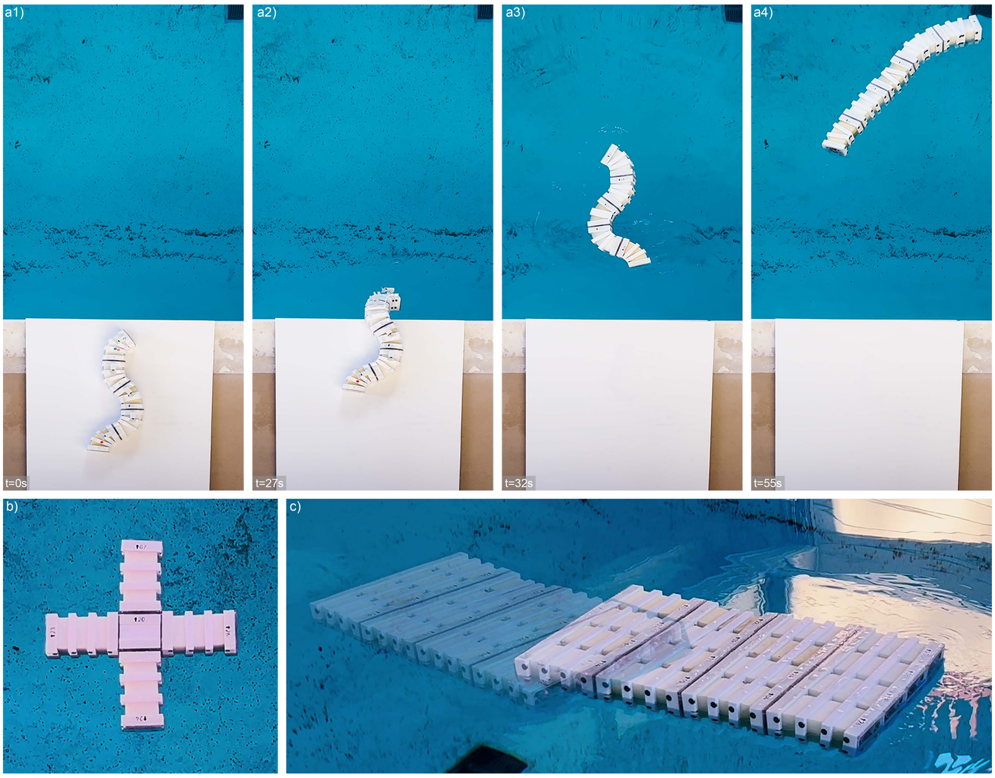

Fig. 7 Examples of locomotion capabilities. (a) Amphibious locomotion inspired by the undulation of a snake. The robot demonstrates snake-like movement on the ground (a1–a2) and utilizes a propeller for locomotion in water (a4). (b) Omni-directional locomotion demonstrated using a cross-shaped (+) configuration, enabling movement in all directions. (c) Lattice locomotion is achieved by actuating the propellers of modular units in different patterns, allowing coordinated movement of the entire structure.

friction. Due to the placement of the propellers, the modules are inverted during ground locomotion, with the propellers positioned on the top side of the chain to avoid interference with the ground.

When the chain of modules transitions into water, the center of mass causes the structure to self-right, flipping over so that the propellers are positioned underneath the body. Once in this orientation, the propellers are activated to provide efficient locomotion in the water, enabling smooth amphibious movement.

This dual locomotion strategy highlights the adaptability of the modular robot system, enabling seamless transitions from ground to aquatic environments. The system leverages different mechanisms for propulsion in each domain, with a self-righting capability ensuring stability and functionality during the transition from ground to water. However, the reverse transition—from water to ground—has not yet been demonstrated and remains a potential area for future exploration.

Omni-directional locomotion in plus-sign configuration

When five modules are assembled into a plus-sign configuration, the middle module is compressed to serve as a connector, linking the four surrounding modules, as shown in Fig. 7(b) and Movie S1 . This configuration enables omnidirectional locomotion, allowing the robot to move in eight different directions by coordinating the actuation of the propellers on the modules, following a thruster-vectored configuration used in several classic underwater remotely operated vehicles. For instance, to move the robot diagonally toward the right-forward direction, the propellers on the left and back modules should rotate in the positive direction, while the propellers on the front and right modules should rotate in the negative direction. This coordinated actuation produces the desired net force to move the robot in the specified direction.

The plus-sign configuration demonstrates the versatility of the modular design, enabling precise control and movement across multiple directions, making it suitable for tasks requiring high maneuverability in dynamic environments.

Discussion

This work demonstrates the versatility and adaptability of aquatic soft modular robots, highlighting their potential to address complex tasks in aquatic environments. The proposed design integrates modularity, softness, and amphibious capabilities, enabling the robots to perform diverse functionalities such as locomotion, manipulation, and structure formation. The ability to transition between soft and rigid states through the combination of rigid and soft foam components allows the robots to adapt to a wide range of tasks, from forming stable structures to performing precise manipulations.

The locomotion strategies demonstrated by the modular robots, including the amphibious undulation gait and the omnidirectional plus-sign configuration, highlight their ability to operate effectively on both ground and water. In addition, manipulation techniques such as caging, grasping, peristaltic motion, and contactless methods showcase their versatility in interacting with objects without traditional grasping mechanisms, providing effective solutions for handling irregularly shaped or fragile items. Beyond locomotion and manipulation, the robots excel in structure formation, creating dynamic assemblies like flat lattices for temporary platforms, such as drone landing pads, or larger lattices for constructing structures like bridges. The ability to reconfigure into various shapes, including chains, plus-signs, and connected lattices, emphasizes the adaptability of the modular design, enabling a broad range of tasks and applications in aquatic environments.

While the results highlight the promise of the system, several limitations must be addressed in future work. The cable-driven actuation system, though lightweight and precise, relies on robust waterproofing measures, such as shaft seals and PMMA covers, which may face durability challenges during extended operation. Additionally, the reliance on propellers for aquatic locomotion introduces constraints in energy efficiency and speed, suggesting the need for alternative propulsion methods, such as bio-inspired fin mechanisms, to improve performance. The connection mechanism, using permanent magnets, provides secure and reliable attachment between modules, unaffected by external forces. However, the current system does not support active detachment between individual modules. Detachment is limited to pre-defined points within a connected chain of modules, which constrains the reconfiguration process. Incorporating an active connection mechanism could enable more efficient attachment and detachment, allowing for greater flexibility in dynamic tasks. Furthermore, as the complexity of control increases with larger configurations, more advanced algorithms will be necessary to optimize coordination and performance. Finally, the structural integrity of modular assemblies, such as lattices and bridges, requires further exploration under real-world dynamic conditions, particularly for validating load-bearing capabilities.

This research establishes a foundation for advancing aquatic soft modular robots by combining modularity, deformability, and amphibious functionality into a single system. Enhancements in durability, propulsion, and control, alongside rigorous field validation, will be crucial for realizing their full potential. These robots hold promise for applications in environmental monitoring, underwater exploration, and disaster relief, offering a modular and adaptable solution for aquatic environments.

Methods

Block fabrication and design

The fabrication of each SoftRaft module combines simplicity, functionality, and adaptability, utilizing lightweight materials and precise manufacturing techniques. The specifications of a single SoftRaft robot are provided in Table. 1, where the weight of a single module is 384 g. The rigid head and tail are 3D-printed using Resin, chosen for its high precision and waterproof feature. The rigid middle parts are 3D-printed using PETG. The PMMA covers is laser cut. The soft foam core is 32D in stiffness, weighs 11 g, and is selected for its buoyancy and flexibility, enabling smooth deformation during transitions between soft and rigid states.

The cable-driven system is powered by an N20 DC motor equipped with a magnetic encoder (12V, 50,000 rpm, 1:100 gear ratio), providing precise control over string lengths for deformation and steering. The propeller motor, used for aquatic locomotion, model FC130BV-13215/42N-R. Each N20 motor weighs 10.9 g, while the whole propeller structure weighs 25.5 g. N35 magnets, embedded for modular connectivity, have a thickness of 3 mm and a diameter of 12 mm, ensuring robust and secure attachment between modules.

Waterproofing measures include silicone glue (TIAN MU® 702) and waterproof grease (YIJIALIN® RUBBER SILICON) for sealing sensitive components. The total weight of the battery (27.5 g), PCB (13.2 g), and other electronic components ensures that each module maintains a lightweight design without compromising functionality. By distributing components between the head and tail sections, we achieve the robot's optimal mass-buoyancy equilibrium.

The circuit and control flow, as shown in Fig. 8, highlight the modular integration of electronic components. The ESP32-S2 microcontroller is used for communication and control. The system is supplied with a 3.7V 903052 1,800 mAh Li-ion battery, converted to three 12V and one 3.3V for operation. The control flow design incorporates motor drivers, power monitors, and sensors such as a Hall effect sensor encoder for

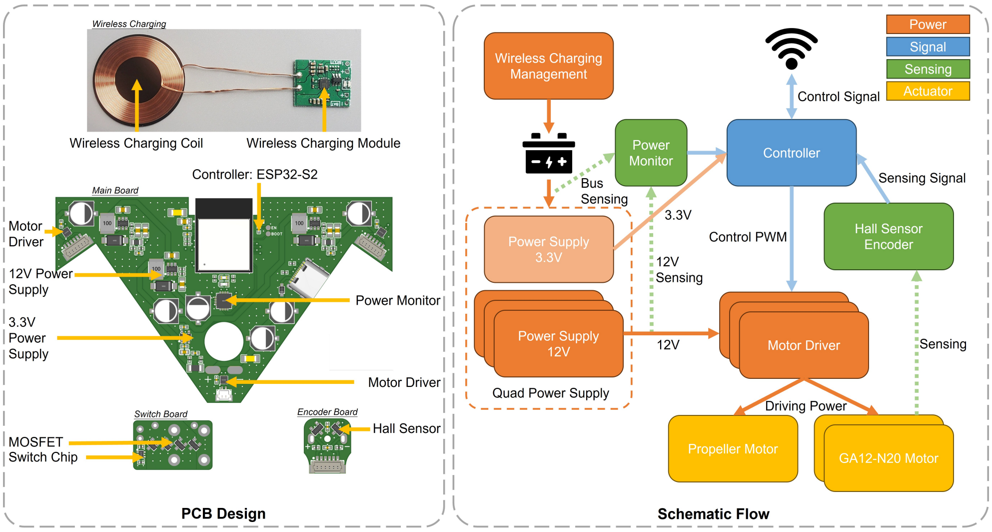

Fig. 8 **The design of PCB and circuit control flow.**

precise actuation feedback. Wireless charging capabilities are integrated using a dedicated coil and charging module, allowing charging without breaking the waterproof sealing.

Experimental design and data analysis

To measure the maximum load capacity of a single robot, four modules are connected in a 2x2 compressed lattice configuration to ensure stability during the test. A rectangular container is placed on top of the structure, and sand is gradually added until the structure is submerged. This process is repeated across five trials, and the maximum load capacity was reported as the average of these experiments.

All application experiments were conducted in a swimming pool under uniform conditions without additional environmental preparation. Robots were connected to a centralized control terminal via Wi-Fi modules. Commands were issued by an operator using a laptop connected to the same Wi-Fi network as the robots. The centralized terminal enabled precise control of individual modules and coordinated actions across multiple robots. All modules were fabricated identically to ensure consistency in experimental results.

To analyze and compare the robot's performance across different gaits (Figure S1), we collected positional and orientational data using a setup involving an AprilTag attached to the top of the robot and a top-mounted camera for tracking. This setup enabled precise measurement of the robot's x, y, and θ values. For each gait, including forward, backward, left_front, right_front, left_back, and right_back, we conducted 35 trials. During these experiments, the robot started from various random initial positions and orientations. Using the recorded changes in distance (Δdistance) and orientation ($\Delta\theta$), we transformed the data into a standardized local reference frame, assuming the robot's initial position and orientation as $(0, 0, 0)$, with the orientation aligned to the x-axis. To ensure the analysis was robust and focused on typical gait behaviors, we filtered the data to remove outliers for each gait, retaining 30 data points that were representative of the robot's performance. The cleaned data was then analyzed to determine cluster centers representing the robot's average behavior for each gait, and these clusters were visualized to illustrate the motion patterns exhibited by the robot.

The control logic for the experiments and kinematic analyses was implemented in Python, while configuration space calculations were performed using MATLAB.

Data availability

All data needed to evaluate the conclusions in the paper are present in the paper or the Supplementary Materials. Computer code is available from the first author and corresponding authors upon request.

References

[1] Bailey, D.R., Dittbrenner, B.J., Yocom, K.P.: Reintegrating the north american beaver (castor canadensis) in the urban landscape. WIREs Water **6**(1), 1323 (2019) https://doi.org/10.1002/wat2.1323

[2] Reid, C.R., Lutz, M.J., Powell, S., Kao, A.B., Couzin, I.D., Garnier, S.: Army ants dynamically adjust living bridges in response to a cost–benefit trade-off. Proceedings of the National Academy of Sciences **112**(49), 15113–15118 (2015) https://doi.org/10.1073/pnas.1512241112

[3] Feinerman, O., Pinkoviezky, I., Gelblum, A., Fonio, E., Gov, N.S.: The physics of cooperative transport in groups of ants. Nature Physics **14**(7), 683–693 (2018) https://doi.org/10.1038/s41567-018-0107-y

[4] Delfour, F., Faulkner, C., Carter, T.: Object manipulation and play behaviour in bottlenose dolphins (tursiops truncatus) under human care. International Journal of Comparative Psychology **30** (2017) https://doi.org/10.46867/ijcp.2017.30.00.16

[5] Murata, S., Kurokawa, H.: Self-organizing Robots vol. 77. Springer, Tokyo (2012). https://doi.org/10.1007/978-4-431-54055-7

[6] Parker, L.E., Rus, D., Sukhatme, G.S.: Multiple mobile robot systems. Springer Handbook of Robotics, 1335–1384 (2016) https://doi.org/10.1007/978-3-540-30301-5_41

[7] Yim, M., Shen, W.-m., Salemi, B., Rus, D., Moll, M., Lipson, H., Klavins, E., Chirikjian, G.S.: Modular self-reconfigurable robot systems [grand challenges of robotics]. IEEE Robotics Automation Magazine **14**(1), 43–52 (2007) https://doi.org/10.1109/MRA.2007.339623

[8] Liang, G., Wu, D., Tu, Y., Lam, T.L.: Decoding modular reconfigurable robots: A survey on mechanisms and design. The International Journal of Robotics Research (2024) https://doi.org/10.1177/02783649241283847

[9] Zhao, L., Wu, Y., Yan, W., Zhan, W., Huang, X., Booth, J., Mehta, A., Bekris, K., Kramer-Bottiglio, R., Balkcom, D.: Starblocks: Soft actuated self-connecting blocks for building deformable lattice structures. IEEE Robotics and Automation Letters **8**(8), 4521–4528 (2023) https://doi.org/10.1109/LRA.2023.3284361

[10] Zhao, L., Wu, Y., Blanchet, J., Perroni-Scharf, M., Huang, X., Booth, J., Kramer-Bottiglio, R., Balkcom, D.: Soft lattice modules that behave independently and collectively. IEEE Robotics and Automation Letters **7**(3), 5942–5949 (2022) https://doi.org/10.1109/LRA.2022.3160611

[11] Jing, G., Tosun, T., Yim, M., Kress-Gazit, H.: An end-to-end system for accomplishing tasks with modular robots. In: Proceedings of Robotics: Science and Systems (2016). https://doi.org/10.24963/ijcai.2017/686

[12] Liu, C., Whitzer, M., Yim, M.: A distributed reconfiguration planning algorithm for modular robots. IEEE Robotics and Automation Letters **4**(4), 4231–4238 (2019) https://doi.org/10.1109/LRA.2019.2930432

[13] Wei, H., Cai, Y., Li, H., Li, D., Wang, T.: Sambot: A self-assembly modular robot for swarm robot. In: 2010 IEEE International Conference on Robotics and Automation, pp. 66–71 (2010). https://doi.org/10.1109/ROBOT.2010.5509214

[14] Zhao, D., Luo, H., Tu, Y., Meng, C., Lam, T.L.: Snail-inspired robotic swarms: a hybrid connector drives collective adaptation in unstructured outdoor environments. Nature Communications **15** (2024) https://doi.org/10.1038/s41467-024-47788-2

[15] Ozkan-Aydin, Y., Goldman, D.I.: Self-reconfigurable multilegged robot swarms collectively accomplish challenging terradynamic tasks. Science Robotics **6**(56), 1628 (2021) https://doi.org/10.1126/scirobotics.abf1628

[16] Paulos, J., Eckenstein, N., Tosun, T., Seo, J., Davey, J., Greco, J., Kumar, V., Yim, M.: Automated self-assembly of large maritime structures by a team of robotic boats. IEEE Transactions on Automation Science and Engineering **12**(3), 958–968 (2015) https://doi.org/10.1109/TASE.2015.2416678

[17] Wang, W., Gheneti, B., Mateos, L.A., Duarte, F., Ratti, C., Rus, D.: Roboat: An autonomous surface vehicle for urban waterways. In: 2019 IEEE/RSJ International Conference on Intelligent Robots and Systems (IROS), pp. 6340–6347 (2019). https://doi.org/10.1109/IROS40897.2019.8968131

[18] Lee, C., Kim, M., Kim, Y.J., Hong, N., Ryu, S., Kim, H.J., Kim, S.: Soft robot review. International Journal of Control, Automation and Systems **15**(1), 3–15

(2017) https://doi.org/10.1007/s12555-016-0462-3

[19] Zhang, C., Zhu, P., Lin, Y., Jiao, Z., Zou, J.: Modular soft robotics: Modular units, connection mechanisms, and applications. Advanced Intelligent Systems **2** (2020) https://doi.org/10.1002/aisy.201900166

[20] Chen, M., Fraddosio, A., Micheletti, A., Pavone, G., Piccioni, M.D., Skelton, R.E.: Analysis of clustered cable-actuation strategies of v-expander tensegrity structures. Engineering Structures **296**, 116868 (2023) https://doi.org/10.1016/j.engstruct.2023.116868

[21] Zhai, Y., Boer, A.D., Yan, J., Shih, B., Faber, M., Speros, J., Gupta, R., Tolley, M.T.: Desktop fabrication of monolithic soft robotic devices with embedded fluidic control circuits. Science Robotics **8**(79), 3792 (2023) https://doi.org/10.1126/scirobotics.adg3792

[22] Mao, Z., Peng, Y., Hu, C., Ding, R., Yamada, Y., Maeda, S.: Soft computing-based predictive modeling of flexible electrohydrodynamic pumps. Biomimetic Intelligence and Robotics **3**(3), 100114 (2023) https://doi.org/10.1016/j.birob.2023.100114

[23] Miriyev, A., Stack, K., Lipson, H.: Soft material for soft actuators. Nature Communications **8** (2017) https://doi.org/10.1038/s41467-017-00685-3

[24] Chung, H.-J., Parsons, A.M., Zheng, L.: Magnetically controlled soft robotics utilizing elastomers and gels in actuation: A review. Advanced Intelligent Systems **3**(3), 2000186 (2021) https://doi.org/10.1002/aisy.202000186

[25] Coyle, S., Majidi, C., LeDuc, P., Hsia, K.J.: Bio-inspired soft robotics: Material selection, actuation, and design. Extreme Mechanics Letters **22**, 51–59 (2018) https://doi.org/10.1016/j.eml.2018.05.003

[26] Li, G., Wong, T.-W., Shih, B., Guo, C., Wang, L., Liu, J., Wang, T., Liu, X., Yan, J., Wu, B., Yu, F., Chen, Y., Liang, Y., Xue, Y., Wang, C., He, S., Wen, L., Tolley, M., Zhang, A.-M., Li, T.: Bioinspired soft robots for deep-sea exploration. Nature Communications **14** (2023) https://doi.org/10.1038/s41467-023-42882-3

[27] Qu, J., Xu, Y., Li, Z., Yu, Z., Mao, B., Wang, Y., Wang, Z., Fan, Q., Qian, X., Zhang, M., Xu, M., Liang, B., Liu, H., Wang, X., Wang, X., Li, T.: Recent advances on underwater soft robots. Advanced Intelligent Systems **6**(2), 2300299 (2024) https://doi.org/10.1002/aisy.202300299

[28] Rich, S.I., Wood, R.J., Majidi, C.: Untethered soft robotics. Nature Electronics **1**(2), 102–112 (2018) https://doi.org/10.1038/s41928-018-0024-1

[29] Yim, M., White, P., Park, M., Sastra, J.: Modular Self-Reconfigurable Robots, pp. 5618–5631. Springer, New York, NY (2009). https://doi.org/10.1007/

978-0-387-30440-3_334

[30] Liljebäck, P., Pettersen, K.Y., Stavdahl, Ø., Gravdahl, J.T.: Snake Robots: Modelling, Mechatronics, and Control. Springer, London (2013). https://doi.org/10.1007/978-1-4471-2996-7

[31] Wright, C., Johnson, A., Peck, A., McCord, Z., Naaktgeboren, A., Gianfortoni, P., Gonzalez-Rivero, M., Hatton, R., Choset, H.: Design of a modular snake robot. In: 2007 IEEE/RSJ International Conference on Intelligent Robots and Systems, pp. 2609–2614 (2007). https://doi.org/10.1109/IROS.2007.4399617

Competing interests: The authors declare they have no competing interests.

Supplementary Materials

This PDF file includes:
Methods
Figures S1 to S2
Tables S1
Other Supplementary Material for this manuscript includes the following:
Movies S1

Supplementary Methods

Kinematics of Modular Robot

In this section, we derive the analytical relationships between the string lengths s_1, s_2, the angle θ, and the length L of the middle curve of a robotic structure. The structure is composed of four rigid 3D-printed components denoted by r_1, r_2, r_3, and r_4, each with length l_r. Figure S2 illustrates the geometric configuration of the structure.

Forward Kinematics: Given s_1 and s_2, find θ and L

The string lengths s_1 (left) and s_2 (right) determine the configuration of the robot. The components $\vec{r}_1$, $\vec{r}_2$, $\vec{r}_3$, and $\vec{r}_4$ are vectors extending from a common point O_1, and the angle θ is the signed angle between $\vec{r}_1$ and $\vec{r}_4$. The vectors $\vec{r}_2$ and $\vec{r}_3$ divide this angle θ into three equal parts. The middle curve of the structure is represented by L, given by $L = 3l_2$, where l_2 is the length of each segment.

When $s_1 \leq s_2$, we derive the following relationships:

Using the triangular similarity principle, the relationship between b, l_r, s_1, and s_2 is given by:

$$\frac{b}{b + l_r} = \frac{s_1/3}{s_2/3}, \quad \Rightarrow \quad b = \frac{s_1 \cdot l_r}{s_2 - s_1}.$$

To determine the angle θ, we apply the cosine rule:

$$\left(\frac{s_1}{3}\right)^2 = b^2 + b^2 - 2b^2 \cos\left(\frac{\theta}{3}\right), \quad \Rightarrow \quad \theta = 3\cos^{-1}\left(1 - \frac{(s_2 - s_1)^2}{18l_r^2}\right). \tag{1}$$

The total length L of the middle curve can be calculated as:

$$L = \frac{s_1 + s_2}{2}. \tag{2}$$

When $s_1 > s_2$, the angle θ becomes negative, and we adjust the formula accordingly:

$$\theta = -3\cos^{-1}\left(1 - \frac{(s_2 - s_1)^2}{18l_r^2}\right), \quad L = \frac{s_1 + s_2}{2}.$$

At the initial state, $s_1 = s_2 = L$, and $\theta = 0$.

Inverse Kinematics: Given θ and L, find s_1 and s_2

To solve for s_1 and s_2 given the configuration parameters L and θ, we use the following relationships derived from equations (1) and (2):

When $\theta \geq 0$, the string lengths s_1 and s_2 are given by:

$$s_1 = L - \frac{1}{2}\Delta s, \quad s_2 = L + \frac{1}{2}\Delta s,$$

where

$$\Delta s = \sqrt{18l_r^2\left(1 - \cos\left(\frac{\theta}{3}\right)\right)}.$$

If $\theta < 0$, swap the values of s_1 and s_2 to reflect the negative angle.

We have derived the relationships between the string lengths s_1, s_2, the angle θ, and the length L of the middle curve of the structure. These relationships provide insights for the kinematic analysis and control of the robotic system.

Supplementary Figures

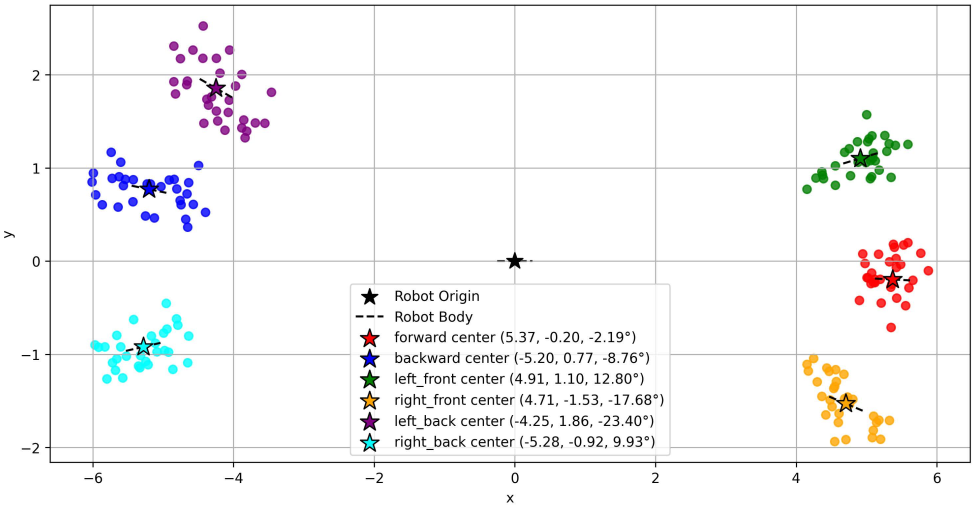

Figure S1: Comparison of x-y positions for different gaits and their corresponding cluster centers with positions and orientations. The figure illustrates the global positions achieved by the robot under six different gaits: forward, backward, left front, right front, left back, and right back. The robot starts at an initial position and orientation of (0, 0, 0), with the initial orientation parallel to the x-axis. Cluster centers for each gait are marked with stars (*), showing their corresponding positions (x, y) and orientations (θ). Dashed lines at each cluster center indicate the robot's body orientation based on the average θ of the gait. The origin (0, 0) represents the robot's starting position, and the dashed black line at the origin indicates its initial orientation.

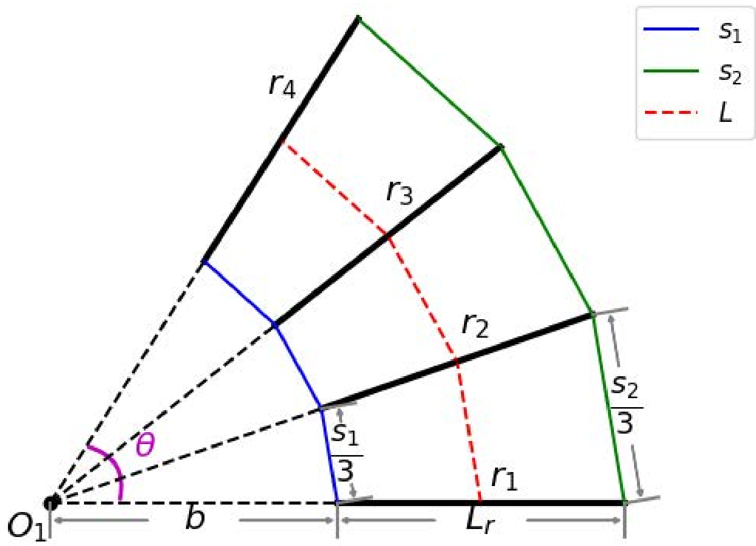

Figure S2: Geometric relationships in the modular robot's kinematics, illustrating the parameters s_1, s_2, θ, and L. The diagram depicts the four rigid components (r_1, r_2, r_3, r_4) extending from a common point O_1, with angle θ divided equally by r_2 and r_3.

Supplementary Table

Table 1 Specs of a single SoftRaft Robot.

Parts	Specification	Parameters	Values
Magnet	2.8 g/unit	Dimensions (original)	200×100×118 mm
Battery	903052 1,800 mAh (27.5 g)	Dimensions (compressed)	100×100×118 mm
SoftRaft rigid components	200.3 g	CoT	68.35
Foam	80×145×60 mm 32D (11 g)	Max swimming speed	0.33 m/s
Motor (cable-driven)	GA-N20 (10.9 g/unit)		
Motor (propeller)	FC130-13215/42N (25.5 g)		
PCB and wires	see Fig. 8 (21.2 g)		
Net weight	384 g		